IEEE Access
Multidisciplinary | Rapid Review | Open Access Journal

Received July 17, 2019, accepted August 22, 2019, date of publication August 28, 2019, date of current version September 12, 2019.

Digital Object Identifier 10.1109/ACCESS.2019.2937992

Doppler Beam Sharpening Using Estimated Doppler Centroid Based on Edge Detection and Fitting

DEQING MAO, (Student Member, IEEE), YONGCHAO ZHANG, (Member, IEEE), YIN ZHANG, (Member, IEEE), YULIN HUANG, (Senior Member, IEEE), AND JIANYU YANG, (Member, IEEE)

West Hi-Tech Zone, Chengdu 611731, China

Corresponding author: Yongchao Zhang (zhang_yongchao1@163.com)

This work was supported by the National Natural Science Foundation of China under Grant 61671117, Grant 61901090, and Grant 61901092.

ABSTRACT Doppler beam sharpening (DBS) technology is widely used in applications, such as helicopter rescue and early warning surveillance. To obtain the desired DBS images with high quality, accurate Doppler centroid estimation (DoCE) is necessary. Conventional methods for Doppler centroid estimation based on navigational devices are sensitive to the errors of the measured motion parameters. Hence, several alternative data-depended approaches have been developed to reduce the error. In this paper, a novel data-depended Doppler centroid estimation method is proposed to improve the image quality of DBS. We begin the method by analyzing the characteristics of range-Doppler distribution in different regions of interests. Then, the edge feature of range-Doppler distribution in forward-looking direction is extracted using morphological filtering and edge detection methods. We will show that the edge feature defines the required Doppler centroid parameters, which can be utilized to estimate the Doppler centroids of the full scene. At last, the estimation error is reduced through fitting the edge with the minimum mean square error (MMSE) algorithm. As compared with conventional Doppler centroid estimation methods, the proposed method can significantly provide reliable estimation accuracy under low echo signal to noise ratio, independent of conditions that strictly required by conventional methods. Simulations and experiments verify the proposed method.

INDEX TERMS Doppler beam sharpening, Doppler centroid estimation, edge detection and fitting.

I. INTRODUCTION

Doppler beam sharpening (DBS) plays a significant role in fields of civil and military applications, such as aircraft self-landing, material airdrop, terrain awareness and avoidance [1], [2]. Often, the DBS technique works with a scanning antenna, and stitches segmented microwave images together, which are obtained with high cross-range resolution using windowed fast Fourier transform (FFT) at each beam position. To achieve this, the knowledge of Doppler centroid is required [3], [4]. Although the Doppler centroids can be estimated by the measured parameters, regrettably, the parameters obtained by the navigational devices suffer from large error as the precision of the navigational devices is usually low, resulting in the decrease of image signal to noise ratio (SNR).

To accurately estimate the Doppler centroid, several data-dependent approaches using echo features in time domain or range-Doppler domain have been well developed [5]–[7]. In time domain, a correlation Doppler estimation (CDE) method is proposed based on the quantitative relationship between the Doppler centroid and the echo correlation function [8]. Compared with the measured parameters by navigational devices (MP) [9], [10], this method can improve the accuracy of Doppler centroid estimation (DoCE). However, the estimation is only can be applied for high SNR. When the SNR becomes low, the echo correlation function is calculated with errors, resulting in degraded precision. In [11] and [12],

The associate editor coordinating the review of this article and approving it for publication was Chengpeng Hao.

a method based on Radon transform is proposed to obtain the estimated Doppler centroid using the relationship between the migration variation and the centroid frequency. However, the method is only suitable for the scene containing strong scatterers, which is the main drawback of the method.

In range-Doppler domain, a peak frequency estimation (PFE) method is proposed because the centroid frequency of a target equips the peak power with high SNR [13], [14]. When the SNR is decreased, the fluctuation of peak power may cause the loss of the contour of the target scene. To avoid the impact of a single frequency on the estimated result, a Doppler centroid estimator based on energy balancing (EB) [15], [16] has been proposed. This method assumes the echo power spectrum distribution within one beam is symmetrical. Therefore, this assumption is only effective to the uniform scene or a point scatterer in squint-looking region [17]. In [18], a minimum-entropy Doppler estimator (MEDE) is proposed depending on the relationship between the DBS image entropy and centroid frequency. This method is able to enhance the scene adaptability, but it is difficult to be applied in large squint-looking region due to the sharp decline of DBS image resolution.

As the DBS usually works for large squint-looking (near on-route direction), and requires both-side imaging, the scanning scope will inevitably covers the forward-looking (on-route) direction. Historically, from the view of imaging, Doppler information in radar forward-looking direction is considered to be useless because of its symmetry of scatterers' distance history and small Doppler gradient. In this paper, we will show that, such Doppler distribution possesses notable edge feature, which defined the required Doppler centroid parameter, independent of the property of the scene, or high resolution, or high SNR. Motivated by the property, this paper proposes a Doppler centroid estimation method based on edge detection and fitting (EDF). To this end, we firstly use morphological filtering to reduce the influence of interfering scatterers. Then, edge detection operator is used to extract the distribution boundary of forward-looking scatterers at different range bins. Finally, the minimum mean square error (MMSE) fitting algorithm is used to smooth the edge. From the fitted edge, the accurate Doppler centroid parameters can be solved, which can be used to estimate the Doppler centroid of scatterers at different positions.

The rest of this paper is organized as follows. In section II, the data model of the DBS is introduced. In section III, the Doppler characteristics for forward-looking and large squint-looking imaging regions are discussed, and the proposed method is illustrated in detail. In section IV, simulations are presented to illustrate the proposed method. In section V, DBS imaging results are listed to testify the superior performance of the resulting method. Section VI contains the conclusion.

II. PROBLEM FORMULATION

The imaging geometry of an airborne radar is illustrated in Fig.1. For the point scatterer $P(\tau,\theta)$, the range history

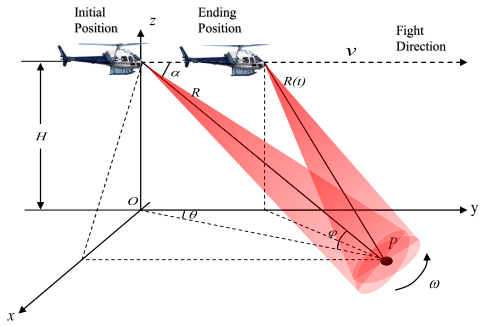

FIGURE 1. Imaging geometry of an airborne radar.

changing over slow time t can be described as [19]

$$R(t)_{(\tau,\theta)} = \sqrt{R^2 + (vt)^2 - 2Rvt\cos\theta\cos\varphi}. \tag{1}$$

where $R = c\tau/2$ denotes the initial range of the scatterer, c the light speed, τ the distance time delay, θ the initial cross-range angle, v the velocity of motion platform, and φ the pitching angle between the radar antenna and scatterer P. The symbol α represents the spatial angle between the radar and scatterer P, namely, $cos\alpha = cos\theta cos\varphi$.

In large squint-looking direction, the range history of target P can be expanded by Taylor series. Because of the short dwelling time of scanning beam, the range history can be further approximately simplified as [20], [21]

$$R(t)_{(\tau,\theta)} \cong R - \cos\theta\cos\varphi vt. \tag{2}$$

Equation (2) shows that the range history can be simplified as linear relationship over slow time in forward-looking direction. Typically, Doppler centroid f_{dc} of a target is defined as the central frequency of the cross-range spectrum within one beam [22]. Assuming that the target is located at (θ, φ), its centroid frequency f_{dc} is expressed as

$$f_{dc} = \frac{2v\cos\theta\cos\varphi}{\lambda} \tag{3}$$

From (3), we can see that the targets located at different azimuth directions equip different Doppler centroids. The targets can be distinguished by narrow band Doppler filters in range-Doppler domain, which is the basic imaging principle of DBS [18], [23].

Generally, the parameters measured by navigational devices may be used to estimate the Doppler centroid of different azimuth. However, in practice, errors of the rough-measured parameters will lead to a large estimation deviation, which deteriorates the image quality of DBS as the wavelength λ is quite small. To overcome this problem, this paper presents a data-depended method to improve the estimation accuracy.

III. PROPOSED EDF-BASED DOPPLER CENTROID ESTIMATION METHOD

To allow for large swath imaging, the antenna continuously scans the region of interest on one side of the flight path or the

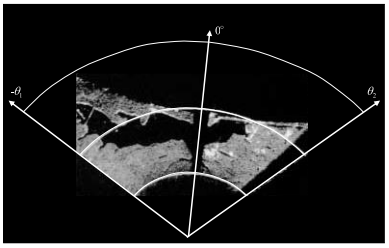

FIGURE 2. Typical DBS imaging mode of an airborne radar in [1].

other, or both. For example, Fig.2 illustrates the typical scanning mode of an airborne radar provided by George W.S. [1], and its scanning scope covers the range from $-\theta_1$ to θ_2 in azimuth. For this reason, the scanning scope will inevitably cover the on-route direction.

In this section, we will show the connection of the Doppler centroid and range-Doppler distribution. Then, the reason why we use the range-Doppler distribution of forward-looking data is illustrated according to the comparison of the distribution properties under varying SNRs. At last, the method is described in detail, and some considerations about the proposed method are given.

A. CONNECTION OF THE DOPPLER CENTROID AND RANGE-DOPPLER DISTRIBUTION

The range-Doppler distribution in this paper refers to the result obtained by transforming the echo data with Fourier transform in azimuth into range-Doppler coordinates.

For a certain target, the Doppler centroid as (3) shows can be transformed as (4) in range-Doppler domain [24].

$$f_{dc} = N * PRF + f_{base} \tag{4}$$

where N represents the Doppler ambiguity number, PRF denotes the pulse repetition frequency, and f_{base} illustrates the baseband Doppler frequency. On the one hand, the Doppler ambiguity number usually estimated by rough-measured parameters or multiple PRF technique [25]. On the other hand, the task of DoCE is converted to estimate the baseband Doppler frequency in range-Doppler domain [26]. Such as the PFE method, which estimates the baseband Doppler frequency according to confirming the frequency of peak power [13], [14]. The EB method estimates the baseband Doppler frequency according to finding the frequency of energy balance [15], [16]. Therefore, the characteristics of range-Doppler distributions provide different ways to estimate the Doppler centroid. In this paper, we utilize the range-Doppler distribution feature of the forward-looking direction to estimate the baseband Doppler frequency.

B. PROPERTIES OF RANGE-DOPPLER DISTRIBUTIONS FOR DIFFERENT DIRECTIONS

In Fig.3, the range-Doppler distributions of different directions under varying SNRs are shown. When the beam center scans the large squint-looking region as the red rectangle

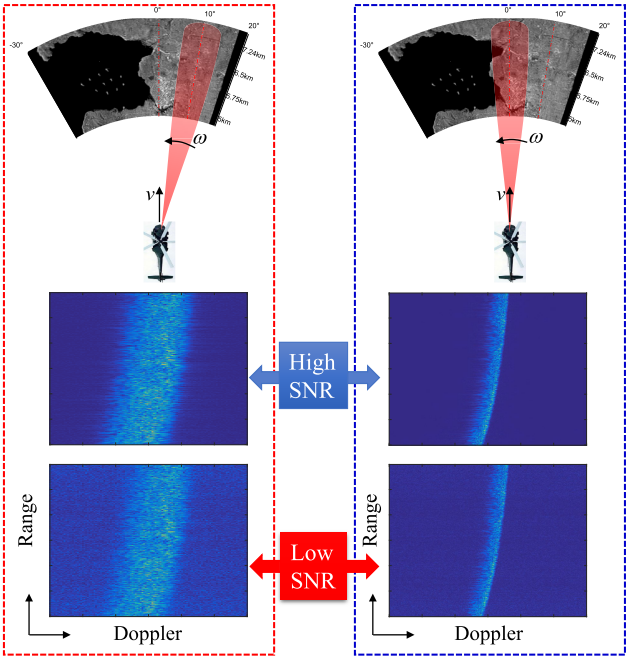

FIGURE 3. Range-Doppler distributions of different directions under varying SNRs.

shows, the range-Doppler distribution within one beam is illustrated as a transitional edge under high SNR. Although the distribution seems to form an edge under high SNR, we cannot accurately determine the angle which it corresponds. Worse, the transitional edge is submerged in the background for the case of low SNR. As a contrast, when the beam center scans the forward-looking direction (0°) as the blue rectangle shows, the range-Doppler distribution are symmetrical, which are folded and overlapped to form a notable edge. Meanwhile, the forward-looking scatterers have the highest Doppler frequency, and no other scatterers in the range-Doppler domain are higher than the 0° scatterers. Even under low SNR $= 5\,dB$, from the comparison, the range-Doppler distribution of the forward-looking direction equips more notable edge than that of the squint-looking direction. The edge characteristic of range-Doppler distribution provides the potential to estimate the Doppler centroid under low SNR. More, such property is independent of the scene, or high resolution, or high SNR.

C. PROPOSED METHOD

In this subsection, the proposed EDF-based Doppler centroid estimation method is described in detail.

1) BINARIZATION AND MORPHOLOGICAL FILTERING

As Fig.4 shows, to acquire the whole range of range-Doppler distribution, the data is binarized at first. The range-Doppler distribution after binarization can be expressed as

$$S_{bw} = \begin{cases} 1, & S \geqslant otsu(S) \\ 0, & otherwise \end{cases} \tag{5}$$

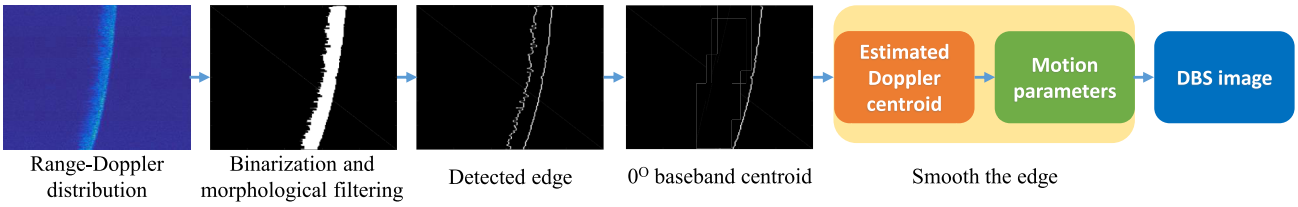

FIGURE 4. Process flow of the proposed method.

where S_{bw} illustrates the range-Doppler distribution of forward-looking direction data after binarization, S denotes the range-Doppler distribution of echo data, and $ostu(.)$ represents the threshold of binarization confirmed by the method of maximum inter-class variance [27].

To reduce the fluctuation of the peak frequency, morphological filtering, such as eroding and dilating operations, is used to smooth the binarized edge. The process can be expressed as

$$I = (S_{bw} \oplus M_e) \ominus M_i \tag{6}$$

where I represents the binarized data after morphological filtering. M_e and M_i denote dilating operator and eroding operator respectively. $\oplus$ and $\ominus$ illustrate the dilating operation and eroding operation respectively.

2) EDGE DETECTION AND EDGE FREQUENCIES CALCULATION

Edge detection methods are widely used in the image and video preprocessing [28], [29]. The methods can be used to obtain distribution edge based on the binarized data after morphological filtering. The process can be expressed as

$$\kappa(I) = [\nabla(I)]_{\max} \tag{7}$$

where $\nabla(\cdot)$ denotes the edge detection operator [29], [30]. $[\cdot]_{\max}$ illstrates to obtain the edge of the targets with the highest Doppler frequency. $\kappa(I)$ illustrates column number of the detected highest Doppler frequency targets.

According to the detected edge position, the baseband centroid frequencies of forward-looking targets in different range bins can be acquired [31]. Based on the principle of FFT operation, the centroid frequency of the baseband is calculated by

$$\hat{f}_{base} = \frac{\kappa(I) \cdot PRF}{N_c} \tag{8}$$

where $\hat{f}_{base} = (\hat{f}_{base1}, \hat{f}_{base2}, \cdots, \hat{f}_{basem}, \cdots, \hat{f}_{baseM})$ represents the baseband centroid frequency of different range bins. The difference of Doppler centroid between different range bins is caused by the change of pitch angle. N_c denotes the number of frequency sampling points by the FFT operation. The Doppler centroid of the forward-looking target can be obtained using the frequencies of the detected edge, but the image contour of the target will be destroyed due to the edge fluctuation, as shown in Fig. 10(a) and Fig. 17(d).

3) SMOOTH THE EDGE BY CURVE FITTING

At last, to maintain the image contour of the targets, the minimum mean square error (MMSE) method [32]–[34] is used to smooth the edge. Using the frequencies of the detected edge, the estimated pitch velocity $(\vec{v}\cos\vec{\varphi})$ of the forward-looking targets at different range bins can be calculated by (3). The fitted velocity $\hat{v}$ and the initial pitch angle $\hat{\varphi}$ of the radar platform can be calculated using the estimated pitch velocity of the forward-looking targets at different range bins, as shown below

$$(\hat{v}, \hat{\varphi}) = \arg\min_{v,\varphi} \left\| (\vec{v}\cos\vec{\varphi}) - v\frac{\sqrt{\vec{R}^2 - (R_0\sin\varphi)^2}}{\vec{R}} \right\|_2^2 \tag{9}$$

where $\vec{R} = (R_0, R_1, \cdots, R_m, \cdots, R_{M-1})$ represents the distance vector of different range bins. By minimizing (9), the accurate motion parameters of the platform can be solved using the data fitting methods. Based on the estimated motion parameters, the Doppler centroids of the targets located at different azimuth directions can be calculated by (3). Compared with the traditional Doppler centroid estimation methods, the proposed method reduces the reliance on strong scattering point targets in the scene. Meanwhile, the method can keep a stable performance even under low SNR because of the notable range-Doppler distribution edge of forward-looking scatterers. The process flow of the proposed method is summarized in Fig.4.

D. METHOD CONSIDERATION

Based on the proposed method above, some necessary considerations are given here.

1) RANGE-DOPPLER DISTRIBUTION SHIFT

In the forward-looking direction, the Doppler centroids of the targets are higher than the PRF typically. The range-Doppler distribution edge may be destroyed because of the cycle shift of Doppler centroid. To avoid the destruction of the edge, the range-Doppler distribution can be shifted to a period of PRF first. The shift value f_{dshift} is usually selected by

$$f_{dshift} = \frac{2v'\cos\theta_{max}\cos\varphi'}{\lambda} \tag{10}$$

where v' and φ' denotes the rough-measured velocity and the platform pitching angle respectively. θ_{max} represents the maximum cross-range angle. Empirically, θ_{max} is chosen as

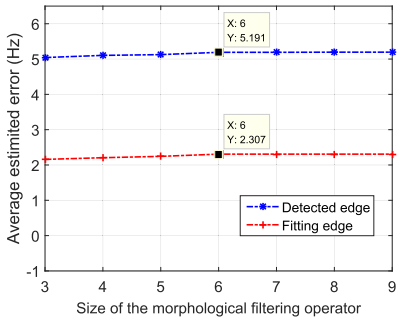

FIGURE 5. Average estimated error of different operator sizes.

θ_β or $2\theta_\beta$, which should be within 10°. In this way, the range-Doppler distribution of forward-looking direction will be kept in a period of PRF.

2) SIZE OF THE MORPHOLOGICAL FILTERING OPERATOR

The style of the morphological filtering operator is various [35]. In the step one of the proposed method, to avoid the influence of special structures on the edge, in this paper, we select the all-one matrix with the dimension $L \times L$ to process the edge. However, the size of the morphological filtering operator should be considered. Using the simulation conditions in section V, the relationship between operator dimension and average estimation error is shown in Fig.5. The average Doppler centroid errors are calculated by

$$f_{dc\_Error} = \frac{1}{M}\sum_{i=1}^{M}\left|(f'_{dc})_i - (f_{dc})_i\right|. \tag{11}$$

where the symbols $(f'_{dc})_i$, $(f_{dc})_i$ represent the estimated Doppler centroid and the ideal Doppler centroid of the ith range bin respectively.

We can find that when the size of the operator is small, the error of centroid estimation is unstable. With the increase of its size, the centroid estimation results tend to be stable. To take account of both operational efficiency and accuracy of centroid estimation result, a small dimension that guarantees stable centroid estimation should be applied. The size of the operator in this experiment is selected as $L = 6$.

IV. METHOD SIMULATION

In this section, some simulation results are given to illustrate each step of the proposed method. The system parameters are listed in Table 1.

A. METHOD VERIFICATION

In Fig.6(a), original scene covers the region $-30° \sim 20°$. Fig.6(b) shows the real beam imaging result of an airborne radar. The cross-range resolution of the real beam imaging is low due to its limited antenna aperture. To compare the proposed method with the CDE method and EB method, in Fig.6, a strong point scatterer T located at (15°, 8 km) is set in the scene.

TABLE 1. System parameters of simulation experiment.

Parameters	Value
Carrier frequency	$X\ band$
Beam width	6 °
Scanning speed	30 °/s
Platform speed	100 m/s
Pitching angle	11.5 °
Signal bandwidth	20 MHz
Pulse width	2 us
1/PRF	250 us
Sampling frequency	30 MHz
Target distance	5 km
Measured speed error	-4 m/s
Measured pitching error	-5 °
Maximum error threshold	0.05 m/s
Signal to noise ratio	5 dB

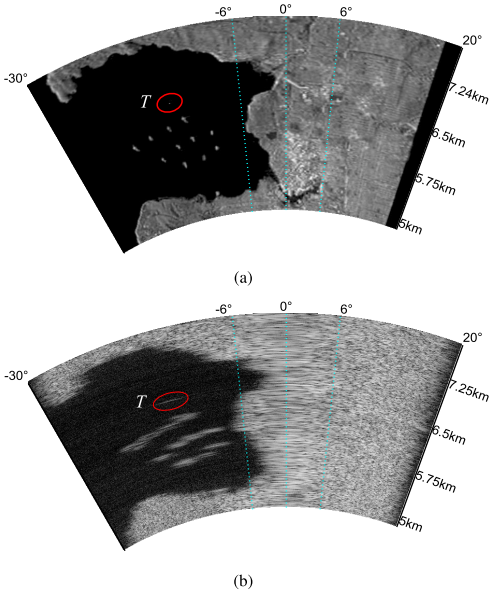

FIGURE 6. Simulation results. (a) Original scene. (b) Real beam imaging.

In Fig.7, the simulation results of each step of the proposed method are given. In this method, the echo data of the forward-looking region $-\theta_\beta \sim \theta_\beta$ is used to estimate the Doppler centroid frequency. The data of $-30° \sim -\theta_\beta$ and $\theta_\beta \sim 20°$ are applied for DBS imaging. Fig.7(a) illustrates the range-Doppler distribution of the forward-looking targets. Due to the narrow Doppler bandwidth and small gradient of forward-looking targets, the edge is more distinct than other regions. Though we can estimate the edge by peak frequency estimation (PFE) directly [13], [14], the target interference will cause the estimation error. Fig. 7(b) is the result of binarization. Fig. 7(c) shows the target distribution after close operation. Fig. 7(d) is the detected target distribution edge. Using the highest frequency edge of Fig. 7(d), the Doppler centroid frequency of each range bin can be calculated, and the fluctuation of edge frequency can be reduced by fitting

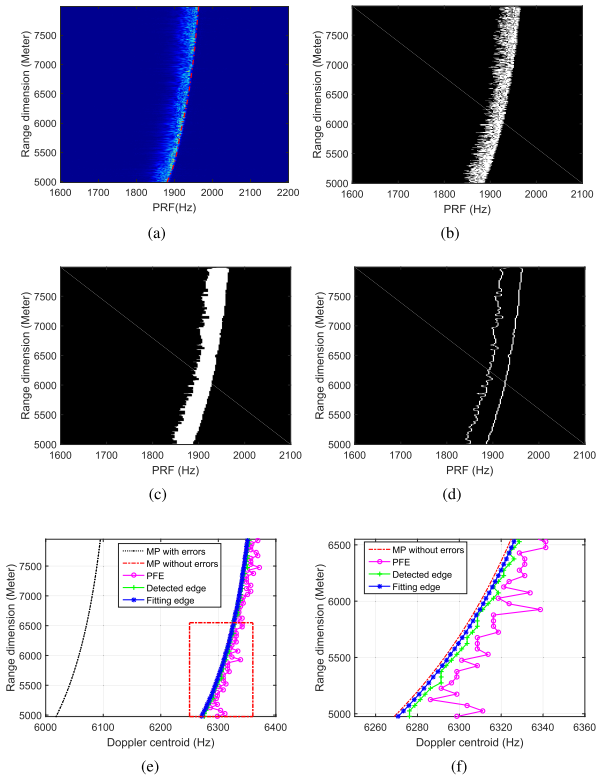

FIGURE 7. Each step of the proposed method. (a) Edge characteristic of the forward-looking targets. (b) Binarization result. (c) Target distribution after close operation. (d) Detected target distribution edge. (e) Estimated Doppler centroid by different methods. (f) Region zoom of estimated f_{dc}.

TABLE 2. Average estimated error of f_{dc}.

Methods	Errors of f_{dc} (Hz)
MP with errors	251.9
PFE	14.1
Detected edge	5.2
Proposed method	2.3

step as shown in Fig. 7(e). Fig. 7(e) gives the results of centroid estimation obtained by different methods. Fig. 7(f) is an enlarged view of the red rectangular area in Fig. 7(e).

From Fig.7(e), we can see that the estimated Doppler centroid is sensitive to the measured motion parameters. When the measured motion parameters are inaccurate as shown in Table 1, the MP method with rough-measured motion parameters exists large error, which will cause targets missing and degrade SNR on the DBS image. To compare the performance of the data-depended methods, in Fig.7(f), the peak frequency of each range bin is fluctuant because of the existing noise jamming. By contrast, the proposed method can reduce the influence of Doppler centroid peak fluctuation by Morphological filtering operation, and the average estimation deviation is reduced by the fitting step. The average Doppler centroid errors estimated by different methods are listed in Table 2.

In Table 2, the average Doppler centroid errors of different data-dependent methods are lower than that of the MP method with errors. Quantitatively, the average Doppler centroid error caused by MP method is 251.9 Hz, and the deviation is excessive to cause a fatal effect on DBS imaging. Using the data-dependent PFE method, the average Doppler centroid error is reduced to 14.1 Hz. Based on the morphological distribution information of the targets, the estimated error is further reduced to 5.2 Hz by edge detection method. In the proposed method, utilizing the relationship between the Doppler centroids at different range bins, the Doppler centroid error is further reduced to 2.3 Hz. From the simulations above, the proposed method can estimate the accurate Doppler centroid of the target using the range-Doppler distribution edge curve of the forward-looking direction, which can improve the image quality of DBS.

B. METHOD COMPARISON

In Fig.8, the Doppler centroid of a strong point scatterer T located at $(15°, 8\ km)$ is compared under different SNRs. Using the Monte Carlo experiments, the estimated centroid is compared under different SNR.

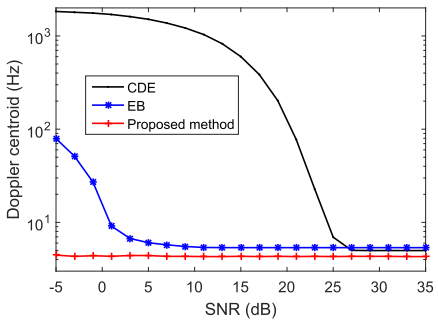

FIGURE 8. Comparison of estimated Doppler centroid under different SNRs.

From Fig.8, the CDE method is sensitive to the echo noise. When the SNR is higher than 25 dB, the three methods can keep a similar performance. When the echo SNR becomes lower than 25 dB, the performance of CDE method is deteriorated sharply. When the SNR is lower than 5 dB, the performance of EB method becomes worse gradually, and the proposed method can keep a stable performance with low SNR.

V. DBS IMAGING BASED ON THE PROPOSED METHOD

Simulations and experimental data are used for DBS to verify the performance of estimated Doppler centroid in this section.

A. DBS IMAGING WITH SIMULATION DATA

Due to the limitation of imaging mechanism, DBS imaging is only suitable for squint-looking areas. As shown in Fig.9(a), the imaging results of sector $-30° \sim -6°$ are given as follows.

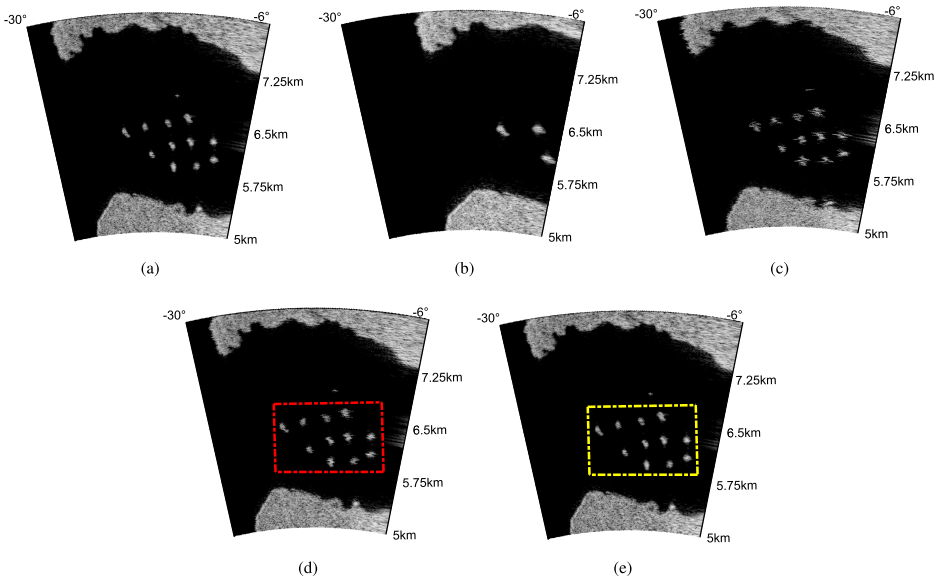

FIGURE 9. DBS imaging by different Doppler centroid estimation methods. (a) Measured parameters without errors. (b) Measured parameters with errors. (c) PFE-based method. (d) The detected edge. (e) The proposed method.

Based on the simulation parameters in Table. 1, Fig. 9 shows the DBS imaging results under different centroid estimation methods. As the original imaging scene and real-beam imaging result shown in Fig. 6(a) and Fig. 6(b), the sector of $-6° \sim 6°$ is applied to estimate the Doppler centroid. Fig. 9(a) shows the DBS imaging result using MP centroid estimation method under error-free condition. It can effectively improve the imaging resolution, but there will be measured errors in actual parameters. Fig. 9(b) shows the DBS imaging result using MP centroid estimation method under error condition. Under this condition, target loss in imaging result is severe because of the large error of Doppler centroid. Fig. 9(c) illustrates a DBS imaging result based on the PFE centroid estimation method. Because of the peak value fluctuation of the centroid, the information loss of the target contour is severe. To reduce the influence of peak fluctuation on centroid, the morphological distribution feature of forward-looking targets is utilized. Fig. 9(d) shows the result of DBS imaging using edge detection method. The loss of contour information is alleviated. However, due to the non-smoothness of the edge, the target contour still suffers a certain loss. Utilizing the relationship between the centroid frequencies of different ranges, the method proposed in this paper can obtain better imaging results based on the fitted edge as shown in Fig.9(e).

To compare Fig. 9(d) and Fig. 9(e) more meticulously, the targets in the rectangular box are enlarged and shown in Fig. 10. We can see that the targets in Fig. 10(a) can be effectively distinguished. Due to the non-smoothness of the detected edge, however, the target contour information suffers a certain loss. Fig. 10(b) is the DBS imaging result of the method proposed in this paper. To evaluate the improvement quantitatively, the image entropy of Fig. 10(a) and (b) are

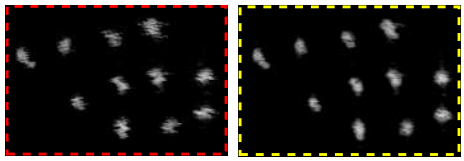

FIGURE 10. Regional comparison of Fig.9. (a) Enlarged region of Fig.9(d). (b) Enlarged region of Fig.9(e).

TABLE 3. The system parameters of real data.

Parameters	Value
Carrier frequency	$X\ \ band$
Beam width	$2.2\ °$
Scanning speed	$5\ °/s$
Measured platform speed	$143\ m/s$
Signal bandwidth	$3.6\ MHz$
Pulse width	$32\ us$
1/PRF	$512\ us$
Sampling frequency	$4\ MHz$
Target distance	$31.6\ km \sim 55\ km$

3.34 and 3.05 respectively. The image contour is completely preserved, and the contour information has important value for target classification and recognition [36], [37].

B. EXPERIMENTAL RESULTS BASED ON REAL DATA

In this subsection, the proposed method is testified by the experimental results based on real data. The experimental parameters are listed in Table.3. In Fig.11, the complete observation region of the real beam data is shown. The real

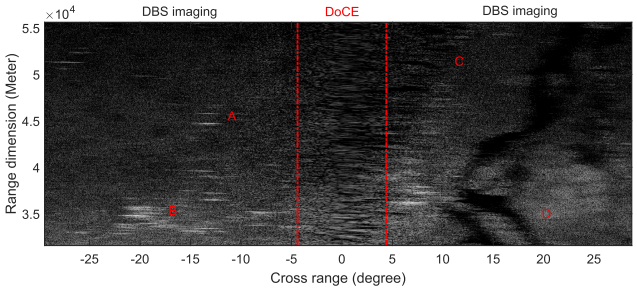

FIGURE 11. Real beam observation.

data contains the region from $-29.5°$ to $28.7°$, where the data covering $-2\theta_\beta \sim 2\theta_\beta$ is applied to estimate the Doppler centroid. The left region $-29.5° \sim -4.4°$ and the right region $4.4° \sim 28.7°$ are used for DBS technique to testify the centroid estimation performance.

To compare different centroid estimation methods, the DBS imaging results of left region $-29.5° \sim -4.4°$ and the right region $4.4° \sim 28.7°$ are given in Fig. 12. The forward-looking region is a dead zone for DBS because of the symmetric Doppler spectrum. In Fig. 12(a), parameter errors lead to incorrect Doppler filters, resulting in low SNR of DBS imaging results and severe loss of target information. In Fig. 12(b), the resolution of DBS imaging based on the PFE method is obviously improved. However, due to the fluctuation of the peak frequency, the contour information of target scene is seriously lost. In Fig. 12(c), the loss of contour information is alleviated, but the image resolution can be further improved. In Fig. 12(d), because the relationship between Doppler centroid frequency and range dimension is considered, the target contour information in the scene is complete, and the targets located at large squint-looking direction can be recovered clearly using the proposed method.

Then, four different regions are selected to quantitatively compare the performance of DBS imaging results. The resolution of real beam in four different regions is relatively low. In region A, a strong scattering target is used to quantitatively verify the improvement of resolution. Regions B, C and D are used to verify the performance of the proposed method to low SNR targets, large squint-looking targets and contour targets, respectively.

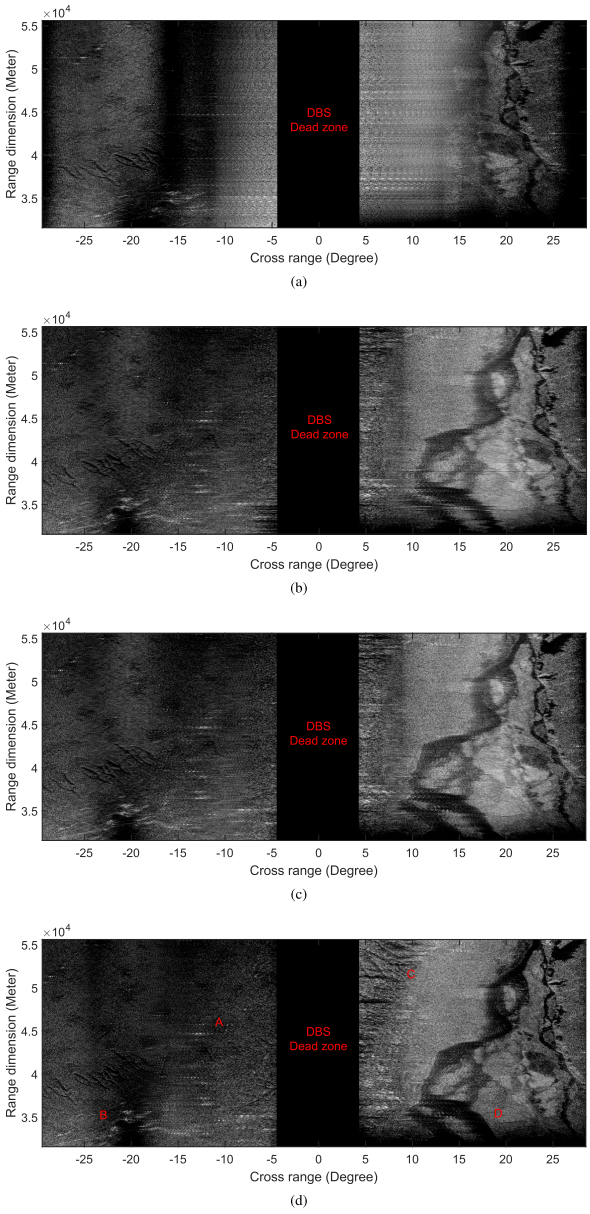

FIGURE 12. Comparison of DBS imaging results. (a) DBS imaging based on MP method. (b) DBS imaging based on PFE method. (c) DBS imaging based on the detected edge. (d) DBS imaging based on the proposed method.

1) REGION A

To quantitatively compare the enhancement of imaging resolution, the imaging results of multi-point targets in region A are given in Fig. 13. In Fig. 13(a), because of the low resolution of the real beam, the imaging results can not distinguish multiple point targets. Although Fig. 13(b) can apparently improve the imaging resolution of multi-point targets, it is impossible to obtain effective information from the imaging results due to Doppler centroid error. In Fig. 13(c), the target blurring problem caused by the widening of the main lobe exists for multi-point targets. In Fig. 13(d), the blurring of multi-point targets is controlled utilizing the centroid parameters obtained by edge detection, but the resolution is still limited. In Fig. 13(e), the imaging resolution of multi-point targets is improved because the proposed method can obtain accurate centroid estimation results.

In Fig. 14, the cross-range imaging profiles of multi-point targets are given to quantitatively calculate the enhancement in resolution. Obviously, the cross-range beam widths of DBS imaging based on data-depended methods are improved compared with the real beam data. Based on the proposed method, the beam width of point target $P1$ is increased by 1.6 times than the PFE method, and increased by 1.75 times

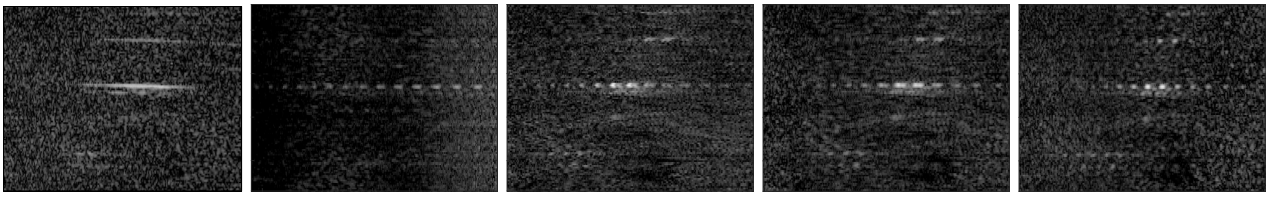

FIGURE 13. Imaging results comparison of region *A* (Multi-point targets). (a) Real beam data. (b) DBS imaging based on MP method. (c) DBS imaging based on PFE method. (d) DBS imaging based on the detected edge. (e) DBS imaging based on the proposed method.

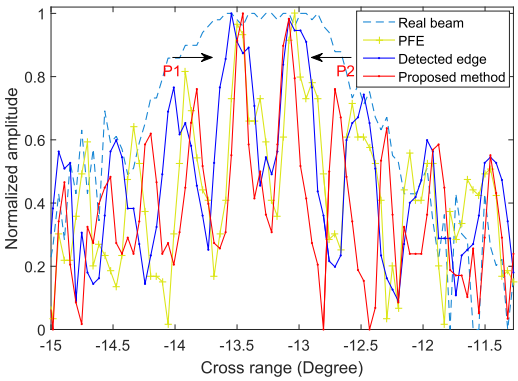

FIGURE 14. Imaging profile of multi-targets in area *A*.

TABLE 4. Image entropy comparison of region *B*.

Figure	Method	Entropy
Figure15(a)	Real beam	4.2181
Figure15(b)	MP	3.9982
Figure15(c)	PFE	3.8984
Figure15(d)	Detected edge	3.9173
Figure15(e)	Proposed method	3.7698

than the edge detection method. For point target *P*2, the cross-range beam width can be improved by 2.0 times than the PFE method, and improved by 1.83 times than the detected edge method.

2) REGION B

Besides strong point targets, the targets of region *B* are compared in Fig.15. The target echo SNR in this region is low. To testify the performance of the proposed method under low SNR condition, the image entropy of imaging results is illustrated quantitatively in Table 4 [18]. As can be seen from Table 4, the image quality of Fig.15(c)-(e) is better than that of Fig.15(a) and Fig.15(b), with lower image entropy. Therefore, the centroid estimation method based on data is obviously superior to the method based on the rough-measured parameters. According to the imaging result in Fig.15(e) and its image entropy, the proposed method performs better imaging quality than that of other traditional estimation methods.

TABLE 5. Image entropy comparison of region *C*.

Figure	Method	Entropy
Figure16(a)	Real beam	4.3056
Figure16(b)	MP	4.6909
Figure16(c)	PFE	4.2810
Figure16(d)	Detected edge	4.2766
Figure16(e)	Proposed method	4.2624

3) REGION C

To further compare the imaging performance in large squint-looking region, the DBS imaging results of region *C* are illustrated in Fig. 16. From Fig. 16(a), we can find that the cross-range resolution of real beam image is low, but ground and ravine information can be observed obviously. Because this region is located in the large squint-looking region, its imaging resolution, which is greatly affected by the accuracy of Doppler centroid, is low due to the small Doppler gradient. Therefore, in Fig. 16 (b)-(d), the scene information is severely lost due to the Doppler centroid error. In Fig. 16 (e), the proposed method can restore rich scene information.

Table 5 gives the image entropy of imaging results in region *C*. As shown in Table 5, the image entropy of Fig. 16(a) is not the worst because of the existence of certain scene texture. In Fig. 16(b), the resolution of DBS imaging deteriorates severely due to the large error of measurement parameters, which makes it impossible to obtain effective information. The image entropy of Fig. 16(b) is worse than that of Fig. 16(c)-(e). From Fig. 16(c) to Fig. 16(e), image entropy is successively improved. Fig. 16(e) has small image entropy and rich image texture.

4) REGION D

Fig. 17 shows the imaging results of region *D* to verify the effect of different centroid estimation methods on scene contours. Scene contour is of great value to scene segmentation and target classification [36], [37]. In Fig. 17(a), the scene contours cannot be obtained because of the low cross-range resolution. In Fig. 17(b), scene information is completely lost in the imaging result based on MP method due to the large error of estimated centroid. In Fig. 17(c)-(e), using the centroid parameters estimated from the echo data, the scene contour can be recovered. In Fig. 17(c), because of the

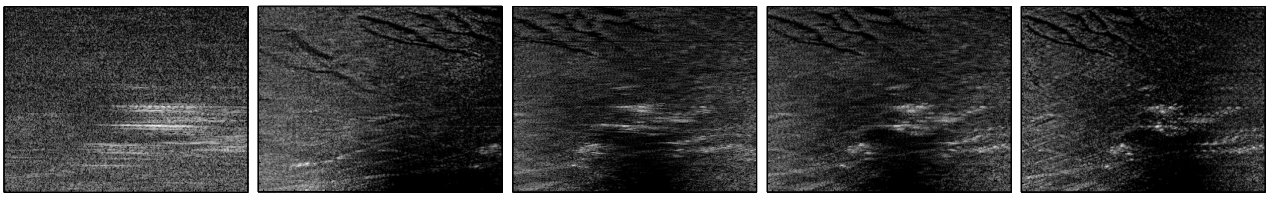

FIGURE 15. Imaging results comparison of region *B* (Low echo SNR). (a) Real beam data. (b) DBS imaging based on MP method. (c) DBS imaging based on PFE method. (d) DBS imaging based on the detected edge. (e) DBS imaging based on the proposed method.

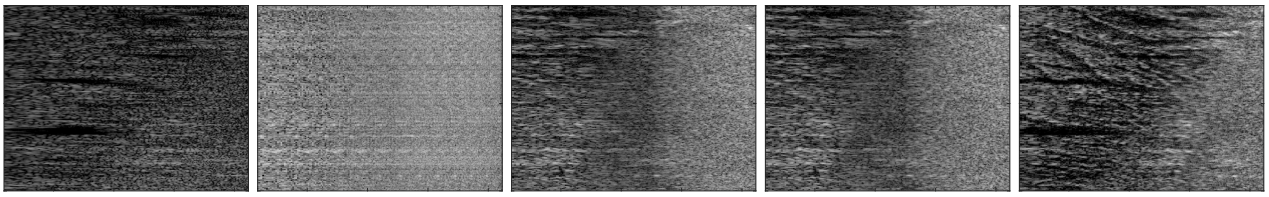

FIGURE 16. Imaging results comparison of region *C* (Large squint-looking). (a) Real beam data. (b) DBS imaging based on MP method. (c) DBS imaging based on PFE method. (d) DBS imaging based on the detected edge. (e) DBS imaging based on the proposed method.

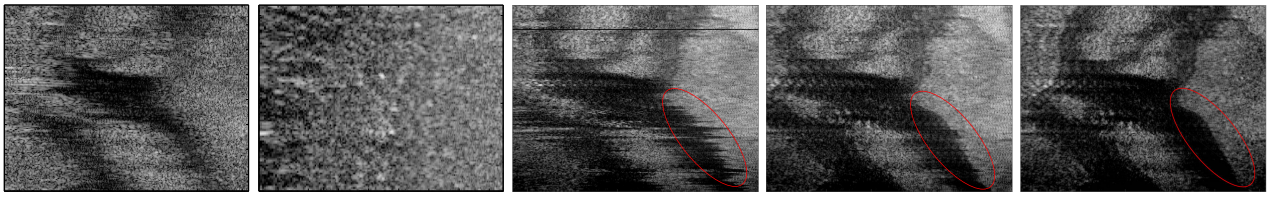

FIGURE 17. Imaging results comparison of region *D* (Scene contour targets). (a) Real beam data. (b) DBS imaging based on MP method. (c) DBS imaging based on PFE method. (d) DBS imaging based on the detected edge. (e) DBS imaging based on the proposed method.

fluctuation of peak frequency, the sawtooth effect appears on the scene edge, which is not favorable to obtain the accurate scene edge. In Fig. 17(d), the scene contour is improved based on the estimated centroid by edge detection method, but there are still errors in the edge. In Fig. 17(e), using the proposed method, the scene contour is smoother and clearer than the other methods mentioned above.

In section IV, simulations are used to verify the performance of different centroid estimation methods. The proposed method can reduce the average Doppler centroid deviation from 251.9 Hz to 2.3 Hz with rough-measured motion parameters. DBS imaging technology is used to verify the performance of the proposed method in this section. Using the above simulations and experimental results, the centroid estimation method proposed in this paper can improve the image quality of DBS in low SNR, large squint-looking region and other scenes under the condition with measurement parameter error. The method can maintain complete image contour and obtain high imaging resolution.

VI. CONCLUSION

In this paper, a DBS method using the estimated Doppler centroid by edge detection and fitting approach is proposed. The method utilizes the relationship between the range-Doppler distribution edge of forward-looking targets and Doppler centroid, estimates the targets' Doppler centroids by edge detection, and reduces the error of estimated centroid by curve fitting. With this method, the resolution of DBS imaging in large squint-looking direction can be effectively improved under low SNR, and the scene contour information is kept completely in imaging mosaic when the motion parameters are measured with errors.

As can be seen from the experiments, the proposed method achieves a stable estimated result under 5 dB SNR. The average estimated error can be reduced from 251.9 Hz to 2.3 Hz, which makes the DBS technology be effective in large squint-looking region. Then, the proposed method is testified using the experimental data.

REFERENCES

[1] G. W. Stimson, *Introduction to Airborne Radar*, 2nd ed. Westchester, CA, USA: Hughes Aircraft, 2014.
[2] M. A. Richards, *Fundamentals of Radar Signal Processing*. New York, NY, USA: McGraw-Hill, 2005.
[3] S.-X. Zhang, J.-L. Sheng, and M.-D. Xing, "A novel focus approach for squint mode multi-channel in azimuth high-resolution and wide-swath SAR imaging processing," *IEEE Access*, vol. 6, pp. 74303–74319, 2018.

[4] M. Y. Jin, "Optimal range and Doppler centroid estimation for a Scan SAR system," *IEEE Trans. Geosci. Remote Sens.*, vol. 34, no. 2, pp. 479–488, Mar. 1996.
[5] W. Yu and Z. Zhu, "Comparison of Doppler centroid estimation methods in SAR," in *Proc. IEEE Nat. Aerosp. Electron. Conf. (NAECON)*, vol. 2, Jul. 1997, pp. 1015–1018.
[6] I. G. Cumming and S. Li, "Adding Sensitivity to the MLBF Doppler Centroid Estimator," *IEEE Trans. Geosci. Remote Sens.*, vol. 45, no. 2, pp. 279–292, Feb. 2007.
[7] M. Yu, J. Xu, and Y.-N. Peng, "SAR PRF-ambiguity resolving by range diversity," *Electron. Lett.*, vol. 41, no. 22, pp. 1246–1247, Oct. 2005.
[8] S. N. Madsen, "Estimating the Doppler centroid of SAR data," *IEEE Trans. Aerosp. Electron. Syst.*, vol. 25, no. 2, pp. 134–140, Mar. 1989.
[9] G. Pietrzyk, P. Samczynski, A. Gorzelanczyk, and K. Kulpa, "Real-time implementation of Doppler beam sharpening technique with simple motion estimation," in *Proc. 1st Eur. Radar Conf. (EURAD)*, Oct. 2004, pp. 185–188.
[10] R.-X. Hu, T. Wang, Z. Bao, and B. Liu, "A novel algorithm for stitching Doppler beam sharpening images based on INS information," *J. Electron. Inf. Technol.*, vol. 34, no. 6, pp. 1337–1343, Aug. 2012.
[11] Y. Kong, B. Cho, and Y. Kim, "Ambiguity-free Doppler centroid estimation technique for airborne SAR using the radon transform," *IEEE Trans. Geosci. Remote Sens.*, vol. 43, no. 4, pp. 715–721, Apr. 2005.
[12] W. Li, J. Yang, Y. Huang, L. Kong, and J. Wu, "An improved radon-transform-based scheme of Doppler centroid estimation for bistatic forward-looking SAR," *IEEE Geosci. Remote Sens. Lett.*, vol. 8, no. 2, pp. 379–383, Mar. 2011.
[13] P. Tortoli, G. Guidi, and V. L. Newhouse, "Improved blood velocity estimation using the maximum Doppler frequency," *Ultrasound Med. Biol.*, vol. 21, no. 4, pp. 527–532, 1995.
[14] R. M. Hardesty, "Performance of a discrete spectral peak frequency estimator for Doppler wind velocity measurements," *IEEE Trans. Geosci. Remote Sens.*, vol. GE-24 no. 5, pp. 777–783, Sep. 1986.
[15] F.-K. Li, D. N. Held, J. C. Curlander, and C. Wu, "Doppler parameter estimation for spaceborne synthetic-aperture radars," *IEEE Trans. Geosci. Remote Sens.*, vol. GE-23 no. 1, pp. 47–56, Jan. 1985.
[16] R. Bamler and H. Runge, "PRF-ambiguity resolving by wavelength diversity," *IEEE Trans. Geosci. Remote Sens.*, vol. 29, no. 6, pp. 997–1003, Nov. 1991.
[17] M. Y. Jin, "Optimal Doppler centroid estimation for SAR data from a quasi-homogeneous source," *IEEE Trans. Geosci. Remote Sens.*, vol. GE-24, no. 6, pp. 1022–1025, Nov. 1986.
[18] T. Long, Z. Lu, Z. Ding, and L. Liu, "A DBS Doppler centroid estimation algorithm based on entropy minimization," *IEEE Trans. Geosci. Remote Sens.*, vol. 49, no. 10, pp. 3703–3712, Oct. 2011.
[19] Y. Zha, Y. Huang, Z. Sun, Y. Wang, and J. Yang, "Bayesian deconvolution for angular super-resolution in forward-looking scanning radar," *Sensors*, vol. 15, no. 3, pp. 6924–6946, Jan. 2015.
[20] Y. Zhang, Y. Zhang, Y. Huang, J. Yang, and W. Li, "Super-resolution surface mapping for scanning radar: Inverse filtering based on the fast iterative adaptive approach," *IEEE Trans. Geosci. Remote Sens.*, vol. 56, no. 1, pp. 127–144, Jan. 2018.
[21] D. Mao, Y. Zhang, Y. Zhang, Y. Huang, and J. Yang, "Super-resolution Doppler beam sharpening method using fast iterative adaptive approach-based spectral estimation," *Proc. SPIE*, vol. 12, no. 1, Mar. 2018, Art. no. 015020.
[22] L. Zhang, Y. Gao, X. Liu, and L. Liu, "A novel method for estimating the baseband Doppler centroid of conventional synthetic aperture radar," in *Proc. IEEE Int. Geosci. Remote Sens. Symp. (IGARSS)*, Jul. 2017, pp. 5426–5429.
[23] H. Chen, M. Li, Z. Wang, Y. Lu, S. Wang, L. Zuo, P. Zhang, and Y. Wu, "Super-resolution Doppler beam sharpening imaging via sparse representation," *IET Radar, Sonar Navigat.*, vol. 10, no. 3, pp. 442–448, 2016.
[24] F. Wong and I. G. Cumming, "A combined SAR Doppler centroid estimation scheme based upon signal phase," *IEEE Trans. Geosci. Remote Sens.*, vol. 34, no. 3, pp. 696–707, May 1996.
[25] C. Y. Chang and J. C. Curlander, "Application of the multiple PRF technique to resolve Doppler centroid estimation ambiguity for spaceborne SAR," *IEEE Trans. Geosci. Remote Sens.*, vol. 30, no. 5, pp. 941–949, Sep. 1992.
[26] S.-S. Zuo, M. Xing, X.-G. Xia, and G.-C. Sun, "Improved signal reconstruction algorithm for multichannel SAR based on the Doppler spectrum estimation," *IEEE J. Sel. Topics Appl. Earth Observ. Remote Sens.*, vol. 10, no. 4, pp. 1425–1442, Apr. 2017.
[27] N. Otsu, "A threshold selection method from gray-level histograms," *IEEE Trans. Syst., Man, Cybern.*, vol. SMC-9, no. 1, pp. 62–66, Jan. 1979.
[28] N. R. Pal and S. K. Pal, "A review on image segmentation techniques," *Pattern Recognit.*, vol. 26, no. 9, pp. 1277–1294, 1993.
[29] G. Shrivakshan and C. Chandrasekar, "A comparison of various edge detection techniques used in image processing," *Int. J. Comput. Sci. Issues*, vol. 9, no. 5, p. 269, Sep. 2012.
[30] N. Kanopoulos, N. Vasanthavada, and R. L. Baker, "Design of an image edge detection filter using the Sobel operator," *IEEE J. Solid-State Circuits*, vol. 23, no. 2, pp. 358–367, Apr. 1988.
[31] D. Mao, Y. Zhang, Y. Zhang, C. Li, Y. Huang, and J. Yang, "Doppler centroid estimation for Doppler beam sharpening imaging based on the morphological edge detection method," in *Proc. IEEE Int. Geosci. Remote Sens. Symp. (IGARSS)*, Jul. 2018, pp. 8925–8928.
[32] Y. Yang and R. S. Blum, "MIMO radar waveform design based on mutual information and minimum mean-square error estimation," *IEEE Trans. Aerosp. Electron. Syst.*, vol. 43, no. 1, pp. 330–343, Jan. 2007.
[33] J. S. Erkelens, R. C. Hendriks, R. Heusdens, and J. Jensen, "Minimum mean-square error estimation of discrete Fourier coefficients with generalized gamma priors," *IEEE Trans. Audio, Speech, Lang. Process.*, vol. 15, no. 6, pp. 1741–1752, Aug. 2007.
[34] T. G. Yadava and H. S. Jayanna, "Speech enhancement by combining spectral subtraction and minimum mean square error-spectrum power estimator based on zero crossing," *Int. J. Speech Technol.*, pp. 1–10, Apr. 2018. doi: 10.1007/s10772-018-9506-9.
[35] J. Serra, "Morphological filtering: An overview," *Signal Process.*, vol. 38, no. 1, pp. 3–11, Jul. 1994.
[36] T. Blaschke, C. Burnett, and A. Pekkarinen, "Image segmentation methods for object-based analysis and classification," in *Remote Sensing Image Analysis: Including the Spatial Domain*. Dordrecht, The Netherlands: Springer, 2004. pp. 211–236.
[37] D. Gokalp and S. Aksoy, "Scene classification using bag-of-regions representations," in *Proc. IEEE Conf. Comput. Vis. Pattern Recognit.*, Jun. 2007, pp. 1–8.

DEQING MAO (S'17) received the B.S. degree from the School of Electronic Engineering, Chengdu University of Information Technology, Chengdu, China, in 2010. He is currently pursuing the Ph.D. degree with the School of Information and Communication Engineering, University of Electronic Science and Technology of China (UESTC), Chengdu.

His research interests include radar signal processing and inverse problem in radar imaging.

YONGCHAO ZHANG (S'15–M'18) received the B.S. degree in electronic information engineering from Hainan University, Haikou, China, in 2011, and the Ph.D. degree from the School of Information and Communication Engineering, University of Electronic Science and Technology of China (UESTC), Chengdu, China, in 2018.

From 2016 to 2017, he was a Visiting Student with Lund University, Lund, Sweden. His research interests include array signal processing and inverse problem in radar applications.

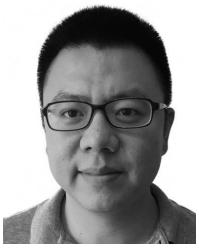

YIN ZHANG (S'13–M'16) received the B.S. and Ph.D. degrees from the School of Electronic Engineering, University of Electronic Science and Technology of China (UESTC), Chengdu, China, in 2008 and 2016, respectively, where he is currently an Associate Professor.

From 2014 to 2015, he was a Visiting Student with the Department of Electrical and Computer Engineering, University of Delaware, Newark, DE, USA. His research interests include signal processing and radar imaging.

YULIN HUANG (M'08–SM'17) received the B.S. and Ph.D. degrees from the School of Electronic Engineering, University of Electronic Science and Technology of China (UESTC), Chengdu, China, in 2002 and 2008, respectively, where he is currently a Professor.

His research interests include radar signal processing and automatic target recognition.

JIANYU YANG (M'06) received the B.S. degree from the National University of Defense Technology, Changsha, China, in 1984, and the M.S. and Ph.D. degrees from the University of Electronic Science and Technology of China (UESTC), Chengdu, China, in 1987 and 1991, respectively, where he is currently a Professor.

His research interests include synthetic aperture radar and statistical signal processing. He serves as a Senior Editor for the *Chinese Journal of Radio Science* and the *Journal of Systems Engineering and Electronics*.